COBEM 2023 27TH INTERNATIONAL CONGRESS OF MECHANICAL ENGENEERING

ABCM Brazilian Society of Mechanical Sciences and Engineering
27th ABCM International Congress of Mechanical Engineering
December 04-08, 2023, Florianópolis-SC, Brazil

COB-2023-0535
FATIGUE CRACK GROWTH IN LASER-TREATED AA2198-T851 ALLOY UNDER ZERO-TO-TENSION LOADING

Cauê P. Carvalho
Gabriel C. C. Peinado
João P. Pascon
Carlos A. R. P. Baptista
Engineering School of Lorena, University of São Paulo (EEL/USP), Estrada Municipal do Campinho, s/n, CEP 12602-810, Lorena-SP, Brazil
caue.pc@usp.br, cotrim@usp.br, jppascon@usp.br, carlos.baptista@usp.br

Milton S. F. Lima
Institute of Advanced Studies, Department of Aerospace Science and Technology (IEAv/DCTA), São José dos Campos/SP, Brazil
miltonsflima@gmail.com

Abstract. *Laser heating treatment (LHT) is a residual-stress-based approach reported to exhibit satisfactory efficiency in enhancing the lifespan of aluminium alloy components. The technique involves local heating followed by fast cooling, inducing compressive residual stresses near this area. As an ongoing technique, the understanding of some questions like how the load ratio R affects the fatigue crack growth (FCG) rate of laser-treated material, their fracture behaviour, and even the influence of microstructural changes remains unresolved. The current study focused on M(T) specimens made of 2.0 mm thick AA2198-T851 alloy sheets with L-T and T-L crack orientations. The specimens were treated with a fibre laser (power 200 W, scanning speed 1 mm/s) to produce heating lines ahead of the crack. Electrical resistance strain gauges were strategically bonded to measure strain during crack growth. FCG tests involved zero-to-tension (R = 0) constant amplitude loading, followed by fractographic analysis using scanning electron microscopy (SEM). Microhardness profiling and X-ray diffraction (XRD) were used to evaluate the influence of microstructural changes on method efficiency. The experimental results indicated significant FCG retardation, particularly in the L-T orientation, in laser-treated specimens. Only LHT specimens showed evidence of secondary cracks, further supporting the FCG retardation effect. The microhardness profile exhibited a decline in a wide range near the heating lines, while XRD analysis revealed the dissolution of certain hardening precipitates. Compared with strain gauge measurements, the results suggest that introduced residual stresses overshadow any potential effects of microstructural changes on FCG.*

Keywords: *laser surface treatment; laser heating treatment; fatigue crack growth; AA2198-T851; fractography*

1. INTRODUCTION

The aeronautical industry is always demanding the development of new alloys in order to achieve improved mechanical properties in lighter materials. Aluminium alloys are well employed in this segment due to their lightweight, high-yield stress achieved due to precipitation hardness, fracture toughness and fatigue resistance, the last two playing an important role in the damage tolerance philosophy adopted by this industry segment (Dursun and Soutis, 2014). Aeronautical application of the lithium addition in aluminium alloys can be traced back to the first generation of Al-Li system, developed during the Cold War era, aiming to weight loss once the alkaline metal is the lighter one in the periodic table. Literature has reported that with the addition of 1% in weight of this element, there is a reduction of 3% in aluminium alloys weight, followed by an increase of 6% in their Young modulus and improvements in the FCG behaviour. In order to enhance the alloy system properties, the third generation arrived in the late 1980s, solving unsettled problems of the former two generations, such as low fracture toughness, high anisotropy and thermal instability (Rioja; Liu, 2012; Alexopoulos et al., 2013; Prasad; Wanhill, 2017). One of the most recent alloys in the Al-Li system is the AA2198, developed to substitute the AA2024 used in aerostructures designed with the damage tolerance philosophy (Sepe et al., 2023). This modern alloy is already being used in aerospace applications as the fuel tank material of the Falcon 9 rocket. It can also be found on the shelves in the aeronautical industry, as the fuselage skin of the Airbus A220, former Bombardier CSeries.

The phenomenon of fatigue also constitutes a significant concern within the aeronautical domain, as it is responsible for approximately 60% of all aircraft service failures (Bhaumik et al., 2008). Beyond that, the aeronautical industry has embraced the damage tolerance philosophy, which necessitates a profound understanding of the fatigue crack growth (FCG) behaviour exhibited by various components. This knowledge is essential for facilitating accurate predictions of

maintenance intervals. Residual-stress-based methodologies have obtained considerable recognition for their ability to prolong the operational lifetime of components, thus leading to a reduction in maintenance expenses.

Two widely employed techniques namely shot peening and cold expansion, have been employed in aircraft manufacturing and maintenance for numerous decades. Shot peening predominantly retards the initiation and early stages of crack propagation through localised plastic deformation resulting from the impact of small particles on the components. Conversely, cold expansion can also retard crack growth in the vicinity of holes by inducing compressive stresses within this region. An alternative residual-stress-based approach, known as laser shock peening, shares similarities with shot peening. However, instead of relying on particle bombardment to induce local plastic deformation, laser shock peening generates plasma expansion through the interaction between the component's material and short-period laser beam irradiation. In comparison to shot peening, laser shock peening exhibits significant promise due to its ability to mitigate concerns regarding surface roughness and its capacity to retard the growth of through-thickness cracks (Sticchi et al., 2015).

In addition to the aforementioned techniques, laser heating treatment (LHT) represents another residual-stress-based approach that has gained considerable attention within the literature due to its considerable potential for retarding FCG (Schnubel et al., 2012; Growth et al., 2015; Cunha and Lima, 2017; Carvalho et al., 2021). The technique was patented by Parker E. and Parker W. (1991) in the early 1990s aiming for aluminium alloy FCG retardation, being later employed in more recent works after a few modifications. The technique consists of local heating followed by fast cooling, which induces residual tensile stresses on the affected area. Although tensile residual stresses present a negative effect on the FCG rate, in the vicinity of the heated area, a compressive residual field is formed, collaborating with the FCG retardation. How the heating occurs locally, the tensile residual stress is contained in a small area in comparison with the compressive one, leading to the beneficial effect of the technique.

Schnubel et al. (2012) evaluated this beneficial effect of LHT on AA2198-T8, the heating was induced in a single continuous line by means of an Nd:YAG laser. As a result, the authors observed on the 5 mm thickness C(T)100 specimens an increase in the lifetime in the order of 300% while treated in comparison with the base metal specimens. Growth et al. (2015) also exhibited the effect of LHT on an aeronautical aluminium alloy, the so-called AA2024-T3. In this work, the authors analysed more reliable and thinner specimens, the 2 mm thickness M(T)200, studying the effect of both single and double pair of treated lines, in continuous and dashed configuration to those lines. The positive effect of the treatment was more prominent for double pair of lines, as for the continuous or dashed configuration of the lines, similar effects were observed.

The current manuscript authors have also studied the positive effect of LHT (Carvalho et al., 2021), for this work a C(T)50 specimen made of a 2 mm thickness AA2198-T851 was employed. Two continuous laser-treated lines were applied by means of the interaction between a Yb:fibre laser beam and the material coated by a thin black graphite layer. The authors' main contribution was on the matter of evaluating the test FCG R-ratio, studying how the treatment effect would be noticed for different R-values. R-ratios of 0.1 and 0.5 were employed, being the treatment's positive effect more prominent on the former. With that, the authors evidenced how the R-ratio is an important factor regarding the treatment's effect analysis, once lower values would reflect a more evident positive effect.

With the aforementioned objective in mind, the present study aimed to assess the impact of a conventional aircraft loading known as zero-to-tension loading (R = 0), which has not yet been examined in the context of LHT applications. The utilized material in this investigation was a 2 mm thick 2198-T851 alloy, employing laser parameters similar to those utilised in prior research (Carvalho et al., 2021). Considering the limitations of C(T) on loading, M(T)50 specimens were applied, also considering that they are more reliable for aeronautical purposes. The laser heating lines were administered in a double-pair configuration, with one pair of lines on each side of the crack front. Concurrently with the FCG test, the strain data of the specimens were measured to monitor their response to the applied loadings during crack growth. This analysis was carried out by means of electrical resistance strain gauges bonded adjacently to the first LHT line on each side of the crack front. This analysis represents early insights into the redistribution of LHT-induced residual stresses as the crack size increases.

Furthermore, attention was given to the examination of microstructural alterations associated with the LHT. This involved assessing the microhardness profile across the thickness of a treated specimen and analysing XRD patterns of a heated line, comparing them to those of an untreated sample. The primary objective of this microstructural analysis was to assess the potential impact of microstructural changes caused by heating on the retarding effect of FCG, rather than exclusively considering the influence of residual stresses. Additionally, fractographic analysis was conducted on both the LHT and as-received (AR) specimens, offering an initial insight into how the treatment influences the fracture behaviour of a specimen subjected to cyclic loading.

2. EXPERIMENTAL PROCEDURES

2.1 Material

The present study utilised the 2198-T851 aluminum alloy to investigate the impacts of LHT. All the analyses were conducted using a 2 mm sheet, whose composition is provided in Table 1. The mechanical properties of the sheet, considering the perpendicular-to-rolling direction, are presented in Table 2.

Table 1. AA2198-T851 composition in weight percent (Al as balance).

Elements	Cu	Li	Si	Fe	Mg	Mn	Ti	Ag	Zr	Zn
% wt.	3.68	1.01	0.03	0.08	0.305	-	0.027	-	0.12	0.01

Table 2. AA2198-T851 perpendicular-to-rolling direction mechanical properties

Yield tensile stress (MPa)	Ultimate tensile stress (MPa)	Young's modulus (GPa)	Poisson's ratio
438.9	480	69	0.35

2.2 Laser heating process

The LHT was directly applied to the FCG specimens using parameters selected from a previous study (Carvalho et al., 2021). The LHT process employed an IPG Photonics Yb: fibre laser, specifically the YLR-2000 model, which had a maximum power output of 2 kW. The treatment was conducted using power and scanning speed parameters of 200 W and 1 mm/s, respectively. The laser beam was defocused and had a focal diameter of 2 mm on the surface of the sample. To ensure the desired interaction, the laser optical head was positioned 12.2 mm above the focal length. A three-axis CNC table was utilised to control the displacement of the specimen. The Z-axis controlled the laser focus, while the X and Y-axes governed the laser position and scanning speed, respectively.

Figure 1 illustrates a schematic representation of the M(T)50 specimen used in the study, along with the configuration of the laser heating lines. The laser heating lines were arranged in two pairs, positioned symmetrically on either side of the crack front. The first lines from each side were situated 11 mm away from the centre of the specimen. The second lines were positioned 4 mm apart from the first lines. To prevent excessive heating, all the lines were 100 mm in length and were centralised on the specimen. These specific configuration details can be observed in Figure 1.

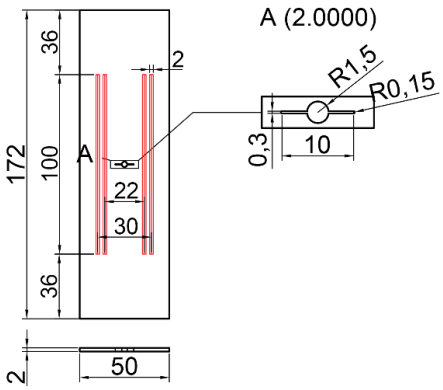

Figure 1. Sketch of the investigated M(T)50 specimen with detail of the notch. Marked in red are the laser heating lines.

2.3 FCG tests

While Schnubel et al. (2012) suggested that laser heating should be employed on T-L-oriented samples due to excessive crack deviation in L-T-oriented ones for the 2198-T8 alloy, the current study aimed to assess this assertion for AA2198-T851. Both L-T and T-L orientations were investigated, involving samples subjected to LHT as well as as-received (AR) samples. To conduct the analysis, FCG tests were performed on M(T)50 specimens, as depicted in Figure 1. The tests were carried out at room temperature in laboratory air, utilising constant load amplitude under force control with an MTS 810 servo-hydraulic machine. The testing procedure adhered to the ASTM E647-15e1 standard. Prior to the tests, a pre-cracking routine was implemented to achieve a 1 mm pre-crack and a final maximum load below the maximum test load. Zero-to-tension tests (R = 0) were conducted, employing a maximum load of 6 kN at a constant frequency of 5 Hz using a sinusoidal loading waveform. The compliance method, specifically employing a clip gage MTS mod. 632.03F-21, was utilised to monitor crack length during the tests. The secant method was employed to convert the crack length (a) versus the number of cycles (N) data into crack growth rate (da/dN) versus stress intensity factor range (ΔK).

During the FCG tests, strain measurements were conducted in the region near the first laser heating lines. The objective was to gather preliminary information about the redistribution of residual stresses resulting from the LHT as the fatigue crack propagated. Half-bridge HBM LY43-0.6/120 linear strain gauges were carefully bonded 9 mm ahead of the theoretical centre of the specimen, on each side of the crack front. These strain gauges had a resistance of 120 Ω and a k-gauge factor of 1.73. The centre of each strain gauge was positioned precisely on the crack propagation line. To ensure sufficient data points, data acquisition was performed at a frequency of 1200 Hz, aiming to capture at least 200 points per loading cycle. The QuantumX MX840A universal amplifier, in conjunction with the catmanEasy software, facilitated the data acquisition process. Data points were acquired every 10,000 cycles, with the interval adjusted as per the observed fluctuations. The mean strain was determined by combining data from the strain gauges on both sides of the crack front. This mean strain value was subsequently utilised in the subsequent steps. Nominal stress-versus-time curves were simulated to align their minima with the strain gauge data, enabling the extraction of hysteresis loops from the test results. By comparing the acquisition cycles with the FCG curves, hysteresis loop data were evaluated for different crack sizes in each specimen. Consequently, a comparison between treated and untreated conditions was feasible for both specimen orientations.

2.4 Fractograpic and microstructural analysis

Following the completion of the FCG tests, the fractured specimens underwent thorough analysis. Due to the symmetry of the samples, only half of each specimen was examined, focusing on only one crack front. To prevent excessive deformation during the sectioning process, a BUEHLER IsoMet 1000 precision saw was utilised. The goal of the fractographic analysis was to study the preserved fracture surfaces of the samples. In contrast, for the microhardness profile and XRD analysis of the treated specimens, additional samples were obtained from the M(T)50 specimens. These were obtained from a region below the fractured surface samples, also avoiding areas with potential laser-induced instability. As for the XRD analysis of the as-received (AR) metal, a sample from the original AA2198-T851 sheet was examined.

The fractographic analysis was specifically conducted on L-T specimens, comparing both the AR and LHT conditions. This choice was made to optimise the analysis by focusing on the condition where the increase in lifetime was most notable. The crack size targeted for investigation ranged between 7.5 and 9.5 mm, with the aim of examining the positive effects of the LHT. It is important to note that this study is preliminary in nature and primarily focused on qualitative analysis; therefore, no statistical investigation was conducted. The fractographic analysis was carried out using a TESCAN field emission gun scanning electron microscope (FEG-SEM) model MIRA4. The secondary electron (SE) detector was utilised to perform the fractographic analysis.

The microhardness profile was specifically obtained for the LHT specimen, as the AR specimen was considered to have sufficiently uniform properties. The cross-section profile of the half M(T)50 specimen was examined to gain insights into how the two laser heating lines affected the material throughout its bulk. The Vickers microhardness profile was conducted using a 50 gf loading and a 10-second dwell time. The indentations were spaced at intervals of 125 μm, following the guidelines outlined in ASTM E384-17, with a safe margin to ensure the stated distance since the average indentation diagonal remained below 30 μm. A similar distance was maintained between the indentations and the edges of the sample. In addition, profiles of the superior and inferior surfaces were also performed and included in the final results.

The XRD analysis involved measurements of both the AR and LHT samples. A Panalytical Empyrean X-ray diffractometer was utilised for this purpose, employing Cu Kα radiation. The measurements were conducted using a step-scanning method within the range of 20° to 90°. Special focus was given to the LHT sample, with the objective of analysing the region affected by the laser heating lines.

3. RESULTS AND DISCUSSION

3.1 FCG tests

Figure 2 depicts the FCG test data for both L-T and T-L specimens under the AR and LHT conditions. Figure 2a illustrates the a versus N curves, while Figure 2b indicates the da/dN versus ΔK curves. Notably, a blue arrow is used in both graphs to indicate a specific point of interest in the LT-LHT specimen, which will be further discussed later.

In Figure 2a, the results clearly demonstrate the significant positive effect of the LHT on the 2198-T851 alloy. Comparing the LHT specimens with their respective AR counterparts in both L-T and T-L orientations, the increase in fatigue life exceeds 300%. This improvement is particularly pronounced in the L-T orientation, where the treated specimen exhibits a lifespan increase of over 650% compared to the non-treated specimen. However, it should be noted that the higher lifetime of the treated L-T specimen alone does not indicate a systematic difference between the two orientations. The blue arrow highlighted in Figure 2a, between 350,000 and 400,000 cycles, supports this observation. It reveals a second plateau in the a versus N curve, suggesting a second delay associated with the residual stresses induced by the LHT technique. It is important to consider that this observation may be more closely related to differences in crack

size between the two crack fronts rather than the orientation itself. Furthermore, it is noteworthy that no significant difference in fatigue life could be observed between the L-T and T-L orientations in the AR condition, further supporting this argument.

In Figure 2b, the plot of fatigue crack growth rate (da/dN) against stress intensity factor range (ΔK) provides additional insights for the ongoing discussion. It reveals that the da/dN values of the treated specimens, before reaching the first heating line, are significantly lower compared to the non-treated specimens (ranging between 10^{-9} and 10^{-8} m/cycle versus 10^{-7} m/cycle). Once the crack propagates beyond the first heating line, both the AR and LHT specimens exhibit a similar trend in da/dN. However, it is important to note that the LT-LHT specimen displays an even higher growth rate after this point, which will be further addressed later.

The observed reduction in crack growth rate before the first heating line is a crucial finding of the LHT technique. It indicates that the FCG retardation associated with the induced residual stresses is only evident in this initial region. Beyond that point, there is no discernible effect of the LHT technique, which could be attributed to the relaxation and redistribution of the aforementioned residual stresses. Furthermore, this observation raises the possibility that the LHT may not be as effective in retarding the growth of larger cracks.

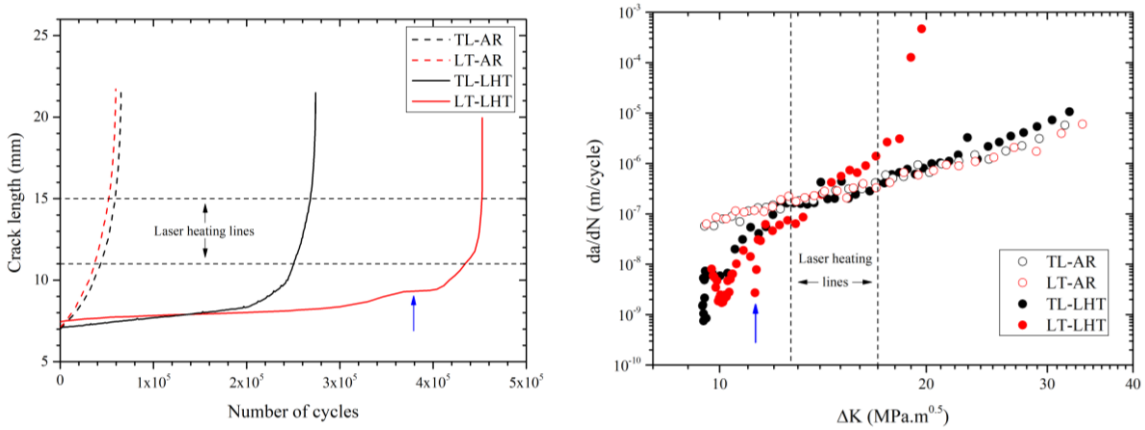

Figure 2. Data from FCG tests of L-T and T-L specimens, for both AR and LHT conditions. (a) Crack length versus the number of cycles; and (b) da/dN versus ΔK curves

Figure 2b provides an opportunity for further development in the discussion, considering the difference in lifetime between the treated specimens as previously mentioned in Figure 2a. Initially, at a stress intensity factor range of around 10 MPa.m$^{0.5}$, the crack growth rates of both specimens fluctuate around similar values, with the TL-oriented sample exhibiting an upward trend and the LT-oriented sample showing a downward tendency. Despite this disparity, one would expect a similar lifespan between the two specimens. However, a second decay in the LT-oriented specimen is observed at a stress intensity factor range of approximately 11.5 MPa.m$^{0.5}$, as indicated by the blue arrow in Figure 2b. This event aligns with the observation made in Figure 2a, where a corresponding crack length is observed.

This second decay in the da/dN value is likely responsible for the observed discrepancy in the lifetime of the treated specimens. As previously mentioned, this phenomenon can be attributed to the difference in crack growth between the two crack fronts of the LT-oriented specimen. Additionally, the rapid increase in crack growth rate after surpassing the first heating line, exceeding the trend observed in the AR samples, provides further evidence to support this premise. The more pronounced delay in one of the crack fronts leads to a loss of structural integrity in the LT-oriented specimen compared to the other specimens when the retarding compressive residual stress field is overcome, resulting in higher da/dN values.

Based on this analysis, it can be inferred that the differences observed between the treated specimens are primarily attributed to the delay in crack growth in one of the crack fronts of the LT-oriented specimen rather than the specimen orientation itself.

3.2 Strain gauge data analysis

In this section, it will be analysed the normal strain at 9 mm from the specimen centre, taking into account different crack sizes. It is important to note that the crack size was indirectly calculated based on the number of cycles, correlating these variables with the a versus N curves shown in Figure 2a. To standardise the crack sizes, approximations were made. This step was necessary to enable a potential correlation between the hysteresis loops of LHT and AR specimens, considering similar crack sizes of 7.00, 7.60, 7.90, and 8.00 mm. However, for the LT-LHT specimen, data for the 7.00 mm crack size could not be obtained, so the 7.50 mm crack size was used as a substitute. Figure 3 illustrates the hysteresis

loops of nominal stress versus normal strain at 9 mm from the centre, comparing the AR and LHT conditions for the respective crack sizes. Figure 3a represents the TL-oriented specimens, while Figure 3b represents the LT-oriented specimens.

In Figure 3, only the maximum nominal stress will be considered for further discussion, as the laser effect is expected to be more prominent when the crack is fully opened. Due to the zero-to-tension loading nature, the minimum normal strain may be affected by crack-closing effects, which could interfere with the analysis.

In Figure 3, an increase in the difference between AR and LHT samples can be observed as the crack size increases. This can be explained by the presence of residual stresses associated with the treatment. The crack tip represents a region of stress concentration, leading to a localised strain field. As the crack grows, the strain near the crack tip affects the measured data. Consequently, larger cracks exhibit higher strain values. As previously discussed in the authors' prior work (Carvalho et al., 2021), the residual stress field resulting from the treatment, combined with the applied test loadings, reduces the normal stress ahead of the crack tip. Therefore, under similar nominal stress conditions, LHT samples exhibit lower normal stress at the crack tip compared to AR samples, resulting in a reduced normal strain measured by the strain gauge.

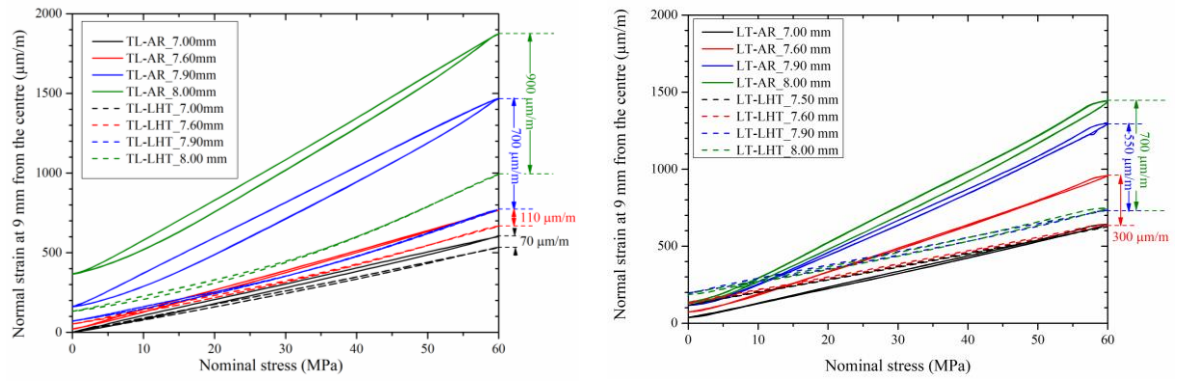

Figure 3. Hysteresis loops evaluating AR and THL conditions for different crack sizes, in which (a) represents TL specimens; and (b) LT ones.

The aforementioned observation is clearly evident in the data. For a crack size of 7.00 mm, the disparity between the maximum normal strain of TL-oriented LHT and AR samples is 70 μm/m. As the crack size increases to 8.00 mm, this difference significantly amplifies to 900 μm/m. A similar trend is observed in LT-oriented specimens, although approximations were made due to the lack of specific data for the 7.00 mm crack in the LT-LHT specimen. By comparing the 7.50 mm data of this sample to the 7.90 mm data, the difference is below 100 μm/m. Therefore, it can be inferred that the difference between the 7.50 mm data and the approximated 7.00 mm data should also be less than 100 μm/m. When considering the overlapping of the maximum normal strain values from the 7.00 mm crack in the AR condition and the 7.50 mm crack in the LHT condition, the difference between the maximum normal strain for both conditions in the 7.00 mm crack becomes smaller, as observed in the TL-oriented specimens. Similarly, this difference progressively increases as the crack size reaches 8.00 mm, reaching a value of 700 μm/m.

It is important to highlight that the observed difference between the AR and LHT conditions is more pronounced in the TL-oriented specimens, providing further evidence that the increased lifetime of the LT-LHT specimen compared to the TL-LHT specimen is primarily attributed to the disparity in the sizes of their respective crack fronts.

In addition to confirming the effectiveness of the laser heating technique, the strain gauge data also offers initial insights into the behaviour of the residual stresses induced by LHT as the crack continues to grow. This information is crucial for future studies involving numerical analysis using the finite element method (FEM).

3.3 Fractographic analysis

Despite efforts to evaluate the effect of laser heating treatment (LHT) on the resulting fracture, no significant difference was observed between the LHT and AR conditions, as shown in Figure 4. Figures 4a and 4b display the 8.00 mm crack in LT-AR and LT-LHT samples at a magnification of 500x. Both figures exhibit similar flat behaviour, with transgranular fractures and multiple layers of macro striations along the crack growth direction, consistent with previous literature findings (Alexopoulos, 2013).

Figures 4c and 4d provide a higher magnification (5000x) of the marked areas in Figures 4a and 4b, respectively. The selected areas aim to highlight the presence of striations. Surprisingly, the treated sample's analysed area shows deeper and more spaced striations compared to the non-treated sample. This observation contradicts the findings from the FCG tests section since striation distance is directly related to the crack growth rate. However, it is important to note that the

da/dN value is calculated based on the mean striation distance of all grains associated with the corresponding crack size, while the presented figures represent the striation distance of only one grain. A more systematic analysis could provide more conclusive results.

Furthermore, it should be noted that the LT-LHT specimen with an 8.5 mm crack size exhibited secondary crack sites, as indicated in Figure 4e. This phenomenon was not observed in the AR condition, which aligns with the findings from the FCG tests study.

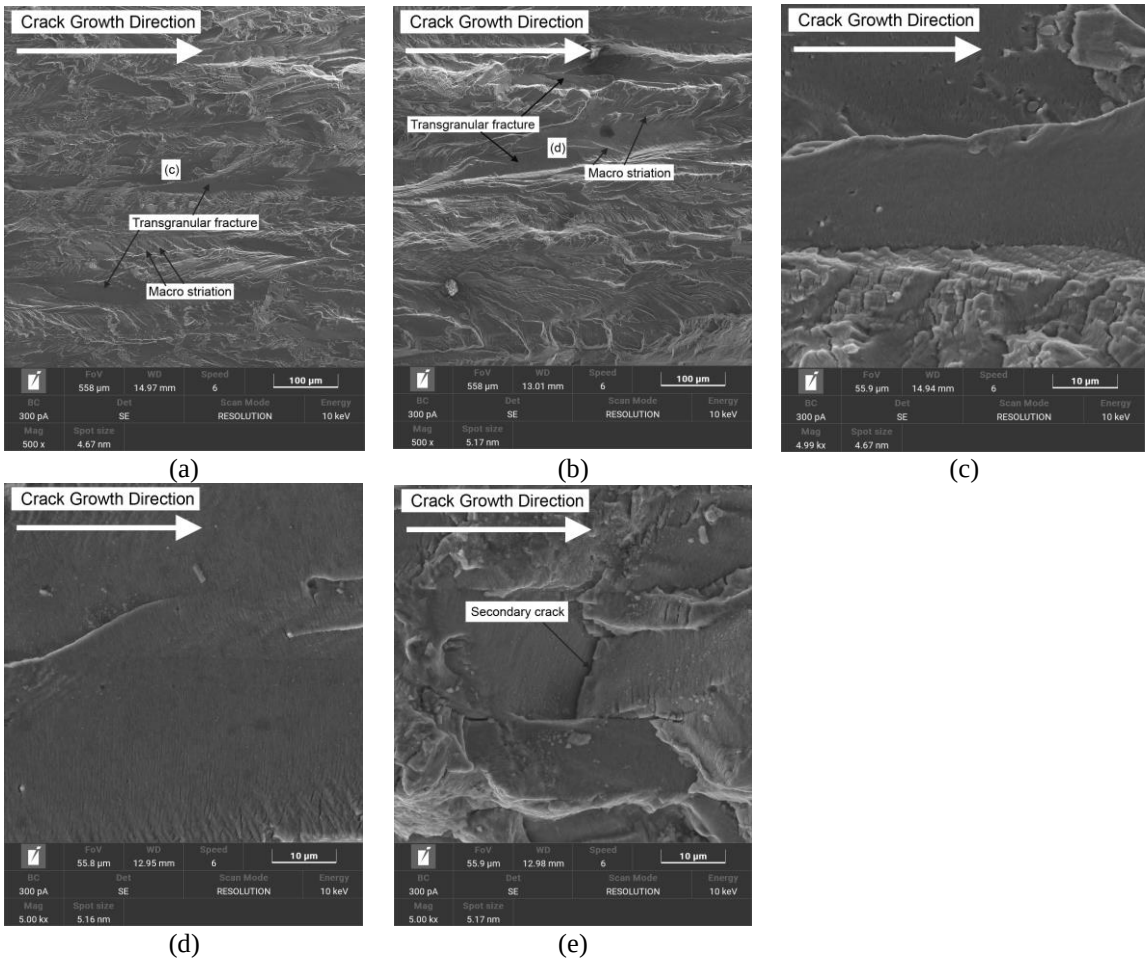

Figure 4. SEM fractography of an 8.00 mm crack of (a-c) LT-AR specimen and (b-d) LT-LHT one, with (a-b) 500x and (c-d) 5000x magnification. (e) Corresponds to an 8.50 mm crack of the LT-LHT specimen with 5000x magnification.

3.4 Microstructural analysis

Figure 5 illustrates the Vickers hardness distribution of the LHT specimen's cross-section. Due to symmetry considerations, only half of the samples were analysed, specifically the area corresponding to one of the crack fronts. The black arrows indicate the specimen's centre and the position where the laser irradiated. In comparison to the original Vickers hardness of approximately 155 HV for the AR condition, it is evident in Figure 5 that the original hardness is only preserved in the region near the specimen's centre (within 5 mm). As the analysed area approaches the laser-irradiation zone, a decrease in hardness is observed. This behaviour was expected, as the mechanical properties of the alloy under investigation are influenced by the precipitation-hardening phenomenon. When the alloy is heated, the hardening precipitates coarsen and/or dissolve, leading to a reduction in material hardness.

The most pronounced effect is observed near the surface, specifically at distances of 11 mm and 15 mm from the specimen's centre, where the heat significantly impacts the entire bulk of the specimen. Additionally, a significant softening is observed in a considerable area ranging from 8 mm to 21 mm. It is important to note that the heating was effective in reducing the hardness even up to the specimen's edge, not restoring the alloy's original hardness near this site.

To provide further insights into the previous observation, Figure 6 is presented, which compares the XRD patterns of the base material (Figure 6a) with the pattern obtained at the laser-irradiation line (Figure 6b). Both patterns exhibit the presence of the same phases, which are typical hardness precipitates in the alloy. These include Al_2Cu (θ or θ'), Al_3Zr (β),

Al_6CuLi (T2), and Al_2CuLi (T1), with the latter being the main contributor to the alloy's mechanical properties. These precipitates have been previously documented in the literature (Lu et al., 2017).

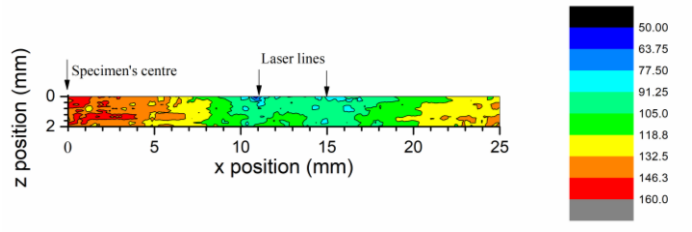

Figure 5. Cross-sectional distribution of Vickers hardness of the LHT specimen.

It is important to note that the δ' phase (Al_3Li) has also been reported in the literature (Donatus et al., 2017). However, its patterns may be overshadowed by the dominant α-Al phase, which is the main phase in this aluminium alloy. Additionally, in the treated area, a graphite carbon peak around 27° is observed, which is associated with residual ablative coating. This finding confirms that the analysed area corresponds to the region that was subjected to laser irradiation.

Given the intensity of the α-Al phase, the scales in Figure 6 were adjusted to display all peaks clearly, minimising background noise. Therefore, no direct comparison was made based on peak magnitudes, as the same phases are present in both patterns. However, new peaks of the θ-phase were observed in the laser-irradiation line area, specifically around 20° and between 45° and 50°. The peaks corresponding to the other phases, which were already visible in the base material pattern, are also present but appear more pronounced in comparison. This observation suggests that the other phases may have been partially dissolved or affected by the laser heating process.

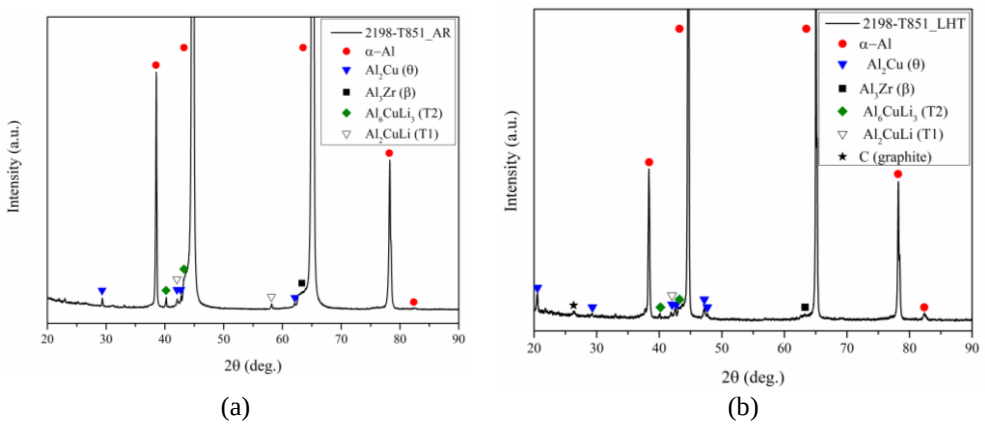

(a) (b)

Figure 6. XRD pattern of AA2198-T851 (a) base material and (b) laser-irradiation line

The correlation between Figure 5 and Figure 6 sheds light on the observed hardness reduction in the treated specimens. The dissolution of some hardening precipitates due to laser heating results in a decrease in hardness. This finding seems contradictory to the hysteresis loops presented in Figure 3, where treated specimens exhibited smaller values of normal strain for similar nominal stress levels. One might expect that the reduced hardness in the treated samples would lead to higher strain values, especially considering that the strain gauge is positioned 9 mm from the specimens' centre, where the reduction in hardness is significant. However, it is crucial to consider the effect of compressive residual stresses induced by the treatment. These residual stresses act to reduce the normal stress values experienced by the material.

Therefore, although the reduction in hardness could potentially increase the normal strain, the dominant effect of the residual stresses outweighs the influence of hardness reduction. In summary, while the microstructural changes resulting from laser heat treatment can influence the fatigue crack growth behaviour in the 2198-T851 alloy, the primary contribution is attributed to the residual stresses induced by the treatment.

4. CONCLUSION

In conclusion, the laser heating treatment has demonstrated its effectiveness in improving the FCG behaviour of M(T)50 specimens of a 2 mm thick AA2198-T851 alloy. This study focused on zero-to-tension loading, which is particularly relevant in the aeronautical field but has not been extensively investigated in relation to the treatment. The orientation of the specimens (LT and TL) did not significantly affect the efficacy of the treatment, as both orientations exhibited a substantial increase in the lifetime of over 300% when treated.

Furthermore, the study revealed that the technique's effect on FCG is primarily observed before the first heating line, indicating that its impact may be more prominent for smaller cracks. However, for larger cracks, the treatment may have a diminished influence. This finding suggests that the laser heating technique is more effective in the early stages of crack growth. Additionally, this work provided initial insights into the redistribution of residual stresses as the crack grows, which could be valuable for future numerical analyses using the finite element method (FEM).

While no conclusive evidence of the technique's influence on fatigue fracture analysis was observed at this stage, further systematic studies are recommended. This includes conducting statistical analyses of the striation distance for different grains at each ΔK value (or crack size). It is also worth noting that the presence of secondary cracks was observed in the treated specimens but not in the AR condition for the same crack size, indicating a potential influence of the treatment on crack propagation behaviour.

The laser heating technique led to a reduction in hardness throughout a significant range from the laser-irradiation sites. This was confirmed by the dissolution of some hardening precipitates observed in the XRD patterns. However, the influence of microstructural changes on FCG was overshadowed by the compressive residual stress field induced by the treatment. Therefore, it can be concluded that the compressive residual stresses are the main contributing factor to the positive effect of the technique.

In summary, this study provides valuable insights into the application of laser heating treatment for improving fatigue crack growth behaviour in AA2198-T851 alloy specimens. Further investigations and analysis are warranted to fully understand the underlying mechanisms and optimise the treatment parameters for different crack sizes and orientations.

5. ACKNOWLEDGEMENTS

This research was funded by the São Paulo State Research Support Foundation (FAPESP), grant number 2018/16438-9. C.P.C. acknowledges the Coordination of Superior Level Staff Improvement (CAPES) and C.A.R.P.B. acknowledges the National Council for Scientific and Technological Development (CNPq) for the research grants.

6. REFERENCES

ALEXOPOULOS, N. D. et al. Fatigue behavior of the aeronautical Al – Li (2198) aluminum alloy under constant amplitude loading. *International Journal of Fatigue*, v. 56, p. 95–105, 2013.

BHAUMIK, S. K.; SUJATA, M.; VENKATASWAMY, M. A. Fatigue failure of aircraft components. *Engineering Failure Analysis*, v. 15, p. 675-694, 2008.

CARVALHO, C. P.; LIMA, M. S. F.; PASTOUKHOV, V.; BAPTISTA, C. A. R. P. Investigation of laser treatment as a method for fatigue crack growth retardation in aluminum alloy 2198-t851. *Metals*, v. 11, n. 12, p. 1–12, 2021.

CUNHA, M. C.; LIMA, M. S. F. The influence of laser surface treatment on the fatigue crack growth of AA 2024-T3 aluminum alloy alclad sheet. *Surface & Coatings Technology*, v. 329, p. 244–249, 2017.

DONATUS, U.; TERADA, M.; OSPINA, C. R.; QUEIROZ, F. M.; BUGARIN, A. F. S.; COSTA, I. On the AA2198-T851 alloy microstructure and its correlation with localized corrosion behaviour. Corrosion Science, v. 131, p. 300-309, 2018.

DURSUN, T.; SOUTIS, C. Recent developments in advanced aircraft aluminium alloys. *Materials and Design*, v. 56, p. 862–871, 2014.

GROTH, A.; HORSTMANN M.; KASHAEV, N.; HUBER, N. (2015), Design of local heat treatment for crack retardation in aluminium alloys. *Procedia Engineering*, v. 114, p. 271–276, 2015.

LU, J.; CHANG, L.; WU, S.; YIN, S. Dendritic Boundary Corrosion of AA2198 Weld Using Fiber Laser Welding with Al–Cu Filler Wire. Acta Metallurgica Sinica, v. 31, p. 735-741, 2018.

PARKER, E. R.; PARKER, W. J. *Method for reducing the fatigue crack growth rate of cracks in the aluminum alloy fuselage skin of an aircraft structure*. U.S. Patent n. 5,071,492, 1991.

PRASAD, N. E.; WANHILL, R. J. H. *Aerospace Materials and Material Technologies*. 1. ed. Singapore: Springer, 2017.

RIOJA, R. J.; LIU, J. The Evolution of Al-Li Base Products for Aerospace and Space Applications. *Metallurgical and materials transactions A*, v. 43, p. 3325–3337, Sept. 2012.

SCHNUBEL, D.; HORSTMANN, M.; VENTZKE V.; RIEKEHR, S.; STARON, P.; FISCHER, T; HUBER, N. Retardation of fatigue crack growth in aircraft aluminium alloys via laser heating – Experimental proof of concept. *Materials Science & Engineering A*, v. 546, p. 8–14, 2012.

SEPE, R.; GIANNELLA, V.; RAZAVI, N.; BERTO, F. Characterization of static, fatigue and fracture behaviour of the aluminium-lithium alloy Al-Li 2198-T851. *International Journal of Fatigue*. v. 166, p. 107265, 2023.

STICCHI, M.; SCHNUBEL, D.; KASHAEV, N; HUBER, N. Review of Residual Stress Modification Techniques for Extending the Fatigue Life of Metallic Aircraft Components. *Applied Mechanics Reviews*, v. 67, p. 1–9, 2015.

7. RESPONSIBILITY NOTICE

The author(s) is (are) the only responsible for the printed material included in this paper.